CrossMark

Raspberry derived mesoporous carbon-tubules and fixed-bed adsorption of pharmaceutical drugs

Shashi Prabha Dubey [a,c,*], Amarendra Dhar Dwivedi [b], Changha Lee [a,**],
Young-Nam Kwon [a,**], Mika Sillanpaa [c], Lena Q. Ma [b,d]

[a] School of Urban and Environmental Engineering, Ulsan National Institute of Science and Technology (UNIST), 100 Banyeon-ri, Eonyang-eup, Ulju-gun, Ulsan 698-805, Republic of Korea
[b] State Key Laboratory of Pollution Control and Resource Reuse, School of the Environment, Nanjing University, Nanjing 210023, China
[c] Laboratory of Green Chemistry, Lappeenranta University of Technology, Sammonkatu 12 (Innovation Centre for Safety and Material Technology, TUMA), 50130 Mikkeli, Finland
[d] Soil and Water Science Department, University of Florida, Gainesville, FL 32611-0290, USA

ARTICLE INFO

ABSTRACT

Novel mesoporous carbon-tubules were prepared from wild plant leaves of *Rubus idaeus* (Raspberry) and their physicochemical characteristics were analyzed by spectroscopic and potentiometric titration methods. The developed carbon-tubules were applied for the aqueous phase decontamination of three pharmaceutical drugs. Ibuprofen, naproxen and clofibric acid were selected for the study. Batch and fixed-bed studies were performed to investigate the adsorption of selected pharmaceutical drugs. Mathematical modelings were applied to the experimental data in order to estimate the maximum adsorption capacity and evaluate the characteristics of the fixed-bed. Based on finding, the adsorption mechanism was investigated by adsorbate and adsorbent physicochemical characteristics.

1. Introduction

Pharmaceutical drugs (PD) and their residues in aquatic environment have attracted concern due to potential endocrine impacts on exposed aquatic organisms [1,2]. They can be persistent and exhibit deleterious effects on organisms [3]. The occurrence of PD in environmental samples and water cycles at trace levels (in range of nanograms to low micrograms per liter) across many countries has been widely discussed in literature in the past decade [4,5]. The occurrence of PD in river water has been investigated in many Asian countries such as Japan, China and South Korea [6–8]. The concentration of ibuprofen (IB) in wastewater effluents in European countries has been reported to vary from 60 to 3400 ng/L [9–14].

Recent investigations for PD removal indicate that sand filtration, flocculation and sedimentation achieve minimal removal efficiency [15,16]. On the other hand, removal or transformations of PD by advanced oxidation technology and adsorption have promising results. Among various water purification and recycling technologies, adsorption is fast, inexpensive and universal [17,18].

Porous activated carbon materials are of great interest in environmental remediation due to their physicochemical properties and activated carbon has thus become a model adsorbent for water contaminants [19]. Despite several advances in carbon synthesis, researchers are continuously exploring the improvement of existing fabrication methods for the development of a new novel carbon. Carbon materials synthesized by conventional methods normally have broad pore size distribution in both micro- and meso-pore ranges [20]. In spite of their extensive applications, microporous carbon suffer a few drawbacks such as slow mass transport of molecules enforced by small pore sizes, low conductivity, and collapse of porous structures at high temperature. To overcome these limitations, efforts have been made to synthesize mesoporous carbon (MC) materials.

In recent years, researchers have synthesized MC for better adsorption of many emerging water contaminants. Sui et al. have studied the rapid removal of bisphenol A on ordered MC [21]. Mesoporous activated carbon was synthesized from solid wastes by Nakagawa et al. [22] for the adsorption of dye. MC was also found effective for pharmaceuticals adsorption and the pore

structure present in carbonaceous material played an important role in pharmaceuticals adsorption [23]. MC was synthesized and used for the adsorption of IB from aqueous solution [24].

In this study, novel MC tubules were prepared using plant *Rubus idaeus* to remove PD with unusual physicochemical characteristics. *R. idaeus* (Raspberry) is native to Europe and northern Asia and commonly cultivated in other temperate regions [25]. Three-component batch and column investigations were performed on derived MC tubules in order to evaluate the influence of the simultaneous presence, which may occur in natural environment. IB, naproxen (NP) and clofibric acid (CA) were considered due to their common occurrence worldwide in river water and wastewater treatment plants (WWTPs) and their consequent high consumption [6,26,27]. In order to understand the adsorption dynamics and solid-liquid phase characteristics of different breakthrough curves, we applied Thomas and Yoon–Nelson models. Mechanistic details were substantially investigated by data of PD adsorption onto MC tubules.

2. Materials and methods

The three pharmaceutical drugs IB, NP, and CA, along with methanol and N,O-bis (trimethylsilyl) trifluoroacetamide (BSTFA), were purchased from Sigma–Aldrich. Ultrapure water was used to prepare the standard solutions. PD solutions at a concentration of 250 mg/L were prepared in methanol and diluted to 10 mg/L with the addition of ultrapure water. The final percentage of methanol did not exceed 0.1% (v/v) in order to prevent any significant influence on the experiment [28]. The different properties of the PD are listed in Table 1.

2.1. Development of RMC

The MC tubules were produced by chemical and physical activation. Raspberry leaves were procured locally during July–August from Mikkeli, Finland. They were washed thoroughly with distilled water to remove traces of particles and to reduce any mineral matter. The leaves were dried and crushed to the 2–4 mm size. Thirty grams of the processed leaves were chemically treated with 50 ml of 80% (v/v) sulphuric acid solution for 8 h. The acid-treated sample was thoroughly washed with ultrapure water until the pH of the solution was within the range of 6.2–6.9, and then dried at 120 °C for 6 h.

The dried carbonized product underwent physical activation for 30 min in a muffle furnace (Carbolite ELF 11/6B, UK) with nitrogen line-up gas flow at a rate 3 °C/min up to 450 °C for gas activation and devolatilization. The material was cooled in a nitrogen gas atmosphere, washed with ultrapure water and finally kept at

120 °C for 6 h for active site homogeneity and stored in a storage bottle at room temperature for adsorption studies. Developed material was named Raspberry mesoporous carbon-tubules (RMC) and characterized for its physicochemical characteristics.

2.2. Physicochemical characterizations of RMC

The surface area, pore volume and pore size of RMC were investigated by N_2 adsorption/desorption-Quantachrome Auto-sorb automated gas adsorption system. The sample was degassed at 350 °C for 3 h prior to adsorption. The pore volume of the MC tubules was calculated from the adsorbed nitrogen after complete pore condensation ($P/P_0 = 0.995$) using the ratio of the densities of liquid and gaseous nitrogen.

The ash content, moisture content and apparent density of the developed RMC were determined by American society for testing and materials (ASTM) guidelines [29]. The surface morphology of RMC was characterized by field emission scanning electron microscopy (FE-SEM, Hitachi, Cold). Energy dispersive X-ray (EDX) and Fourier transform infrared spectroscopy (FTIR 8201 Shimadzu spectrometers) were used to determine the chemical compositions and surface functionalities of RMC. The FTIR spectra were collected within 500–4000 cm^{-1}. Potentiometric titration at different pH levels was conducted to determine the charge and pH$_{zpc}$ of the RMC surfaces by Malvern Zetasizer. The solution pH was set using 0.1 N HCl and 0.1 N NaOH electrolytes.

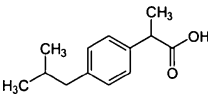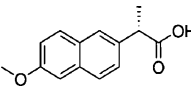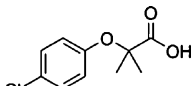### 2.3. PD quantification and adsorption studies

The remaining concentration of PD in aqueous solution was extracted by solid phase extraction method. The extracted sample was derivatized using BSTFA and quantified by Agilent GC-FID. More details can be found in the supplementary data.

Batch adsorption of IB, NA and CA on RMC was conducted at various contact times, pH levels and PD concentrations to evaluate the adsorption parameters. The solution pH was varied from 3 to 9 using 0.1 N HCl and 0.1 N NaOH solution. First, 35 mg of RMC was added in 20 ml of 10 mg/L of solutions in 50 ml stoppered conical flask in an incubator shaker for 5 h at 150 rpm and at 30 ± 1 °C. Then, the samples were filtered using a syringe with 0.45 μm polypropylene filters. The remaining concentration of adsorbate retained in the adsorbent phase was calculated by Eq. (1):

$$q_e = \frac{(C_0 - C_e)}{M_{RMC}} \tag{1}$$

where q_e (mg/g) is the equilibrium adsorption capacity, C_0 and C_e are initial and equilibrium adsorbate concentration (mg/L) and M_{RMC} is amount of RMC added in solution (g/L).

Table 1
Properties of the selected pharmaceutical drug compounds.

Parameters	Ibuprofen	Naproxen	Clofibric acid
Chemical formula & IUPAC Name	$C_{13}H_{18}O_2$ (*RS*)-2-(4-(2-methylpropyl) phenyl) propanoic acid	$C_{14}H_{14}O_3$ (+)-(*S*)-2-(6-methoxynaphthalen-2-yl) propanoic acid	$C_{10}H_{11}ClO_3$ 2-(4-Chlorophenoxy)-2-methylpropanoic acid
Structure			
CAS No.	15687-27-1	22204-53-1	882-09-7
Molecular weight (g/mol)	206.29	230.27	214.6
Aqueous solubility (mg/L)	21.0	15.9	583.0
Log K_{ow}	3.97	3.18	2.57
pK_a	4.91	4.15	3.0
Use	Antiphlogistic	Antiphlogistic	Lipid regulator

The fixed-bed experimental set-up consisted of an Econo column of 1.0 cm ID and 10.0 cm length, which was filled with RMC bed. In order to assure that no flow or movement of adsorbent occurred inside the column, the bed was washed and dried. The volumetric feed flow rates (1.5 and 3.0 ml/min) were varied and maintained throughout the experiments using a peristaltic pump. The PD solutions were passed in down-flow mode through the RMC bed at different bed heights (1.5 and 3.0 cm) and concentrations in the range of 10–20 mg/L.

2.4. Modeling of fixed-bed adsorption

The PD adsorption on the RMC surfaces was described using the two most widely used adsorption models: Thomas model [30] is mostly used for the calculation of maximum adsorption capacity of adsorbent and Yoon–Nelson model [31] give assumption of 50% adsorbate breakthrough time.

2.4.1. Thomas model

One of the most widely used models was developed by Thomas in 1944 and is used to predict breakthrough parameters [30]. The adsorption capacity of the adsorbent can be calculated by the Thomas model, which is helpful in the successful design of the adsorption process [32]. The nonlinear expression of the Thomas model for fixed-bed adsorption is given as [33]:

$$\frac{C}{C_0} = \frac{1}{1 + \exp[(k_{th}q_0m/\upsilon) - k_{th}C_0t]} \quad (2)$$

where k_{th} is the Thomas rate constant (ml/min.mg), q_0 the equilibrium PD uptake per g of adsorbent (mg/g), m the amount of adsorbent (g), υ the volumetric flow rate (ml/min) and t the time in minutes. The Thomas parameters k_{th} and q_0 can be determined using nonlinear regression by plotting C/C_0 versus t.

2.4.2. Yoon–Nelson model

The decrease in adsorption probability for an adsorbate molecule is directly proportional to the adsorbate adsorption and adsorbate breakthrough on the adsorbent surface [31]. This model does not require the details of the type of adsorbent, characteristic of adsorbate or physical properties of the fixed-bed. The Yoon–Nelson nonlinear equation is expressed as [33]:

$$\frac{C}{C_0} = \frac{1}{1 + \exp[k_{yn}(\tau - t)]} \quad (3)$$

where k_{yn} is the Yoon–Nelson rate constant (ml/min), τ the time required for 50% adsorbate breakthrough (min) and t the

Table 2
Physicochemical properties of RMC.

Properties	Results
Surface area (m²/g)	224.6
Pore volume (cc/g)	0.129
Pore size (nm)	2.31, mesoporous material
Ash content (%)	4.78
Moisture content (%)	4.66
Apparent density (g/cm³)	0.656
pH$_{zpc}$	5.48
SEM surface morphology	Carbon-tubules
EDX (elemental composition in %)	C-70.45; N-7.82; O-16.75; S-1.62

breakthrough time in minutes. The parameters k_{yn} and τ can be determined using nonlinear regression by plotting C/C_0 versus t.

3. Results and discussion

3.1. Characterization of RMC

The elemental composition, moisture content, ash content, apparent density, and pore size of the RMC were analyzed and the results are summarized in Table 2. The low ash content (4.78%) indicates the overall activity and efficiency of the material. The surface morphology of the RMC was revealed by SEM and is presented in Fig. 1(a and b). SEM micro images of different particles in the solid mixture gave an impression of carbon-tubules with a pore size (2.31 nm) of a mesoporous material range (i.e., 2–50 nm).

The pH$_{zpc}$ value was 5.48. The surface functionality of RMC was characterized using IR spectroscopy and the possible functional characteristics were assigned and are summarized in Table 3. The potentiometric titration plot of pH vs. zeta potential (mV), FTIR and EDX spectra of RMC are presented in supplementary data (Fig. S1a–c).

3.2. Batch experiments

The batch adsorption of the three PD solutions on RMC was conducted at different contact times and 5 h was considered as the equilibrium time because the adsorption capacity did not change significantly after 5 h. The effect of the initial concentration of the PD solution on adsorption was observed at the optimized equilibrium time. The Langmuir–Freundlich model was found to best represent the equilibrium data among Langmuir, Freundlich, and Langmuir–Freundlich isotherm models (data not shown), suggesting heterogeneous surface adsorption of PD on RMC surface. The isotherm parameters and maximum adsorption
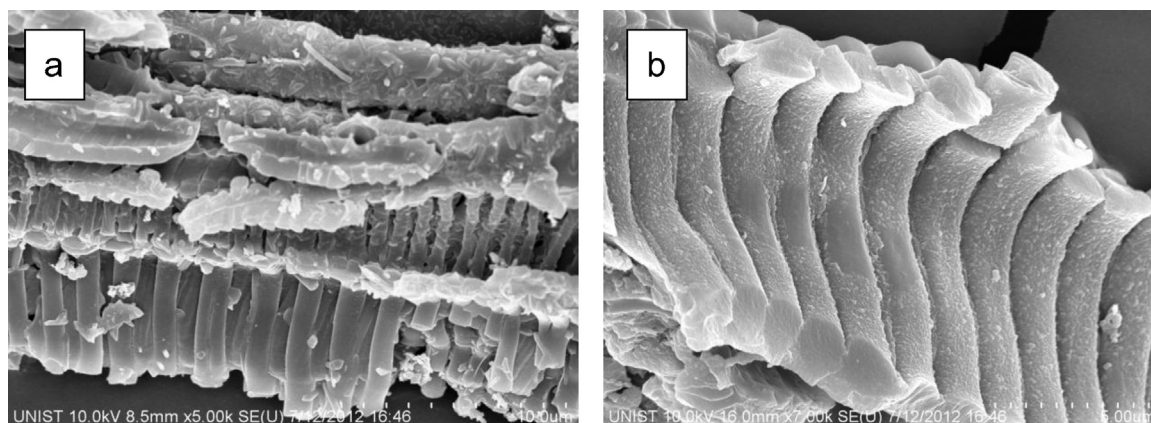

Fig. 1. (a and b) SEM images of carbon-tubules.

Table 3
Surface IR frequency characteristics of RMC.

Observed peak(s) (/cm)	Bond-type	Surface functional group(s) type
3386$_{(s,br)str}$	$\equiv$OH	Phenolics
2918$_{(s,m)str}$	$\equiv$C–H	Aliphatic hydrocarbons
2849$_{str}$		
2160$_{(w;\ small\ but\ exposed)str}$	$\equiv$C=C–C=	Conjugated diene
1977$_{(w)str}$	$\equiv$C–H	Phenyl substitution overtones
1608$_{(s,m)str}$		
757$_{(w)bend}$	$\equiv$C–H	Phenyl ring substitution band
1441$_{(v)str}$	$\equiv$C=C	Aromatic rings
1700$_{(w)str}$	C=O	Ketones
1179$_{(m)str}$	$\equiv$C–O	Aldehyde
1035$_{(m)str}$	$\equiv$C–O	
1329$_{(m)str}$	$\equiv$C–N	Amines

s: Sharp; br: broad; w: weak; m: medium; v: variable; str: stretching.

Table 4
Langmuir–Freundlich isotherm parameters.

Isotherm	Parameters	IB	NP	CA
Langmuir–Freundlich	q_m	22.672	17.712	9.744
	k	0.078	0.066	0.060
	n	1.833	1.167	1.543
	R^2	0.998	0.979	0.981
	χ^2	0.134	0.533	0.254

capacity of RMC at varying initial PD concentrations was obtained from Langmuir–Freundlich isotherm curve (Fig. 2). The estimated isotherm model parameters and correlation coefficients are presented in Table 4.

3.3. Fixed-bed PD adsorption

The adsorption dynamic properties such as the effect of flow rate, bed height and initial pharmaceutical concentration on the breakthrough curve were evaluated. The total adsorption in the column for a specific feed concentration was equal to the area under the breakthrough curve.

The effects of initial concentration on PD adsorption were observed. The breakthrough curves were obtained at different initial PD concentrations from 10 to 20 mg/L at 1.5 ml/min flow rate on 1.5 cm RMC bed. Fig. 3 shows the breakthrough curves at different initial PD concentrations for IB, NP, and CA, respectively. In all the cases, the breakthrough time decreased with increasing initial concentration due to the rapid saturation of the active binding sites available on the RMC surfaces at higher initial feed concentrations. Breakthrough occurred after 840 and 180 min at initial IB concentration of 10 and 20 mg/L, after 540 and 120 min at initial NA concentration of 10 and 20 mg/L and after 420 and 120 min at initial CA concentration of 10 and 20 mg/L, respectively.

The flow rate for PD adsorption was varied from 1.5 to 3 ml/min, while the initial PD concentration and bed height were kept constant at 10 mg/L and 1.5 cm, respectively. The breakthrough curves at different flow rates for IB, NP, and CA adsorption are
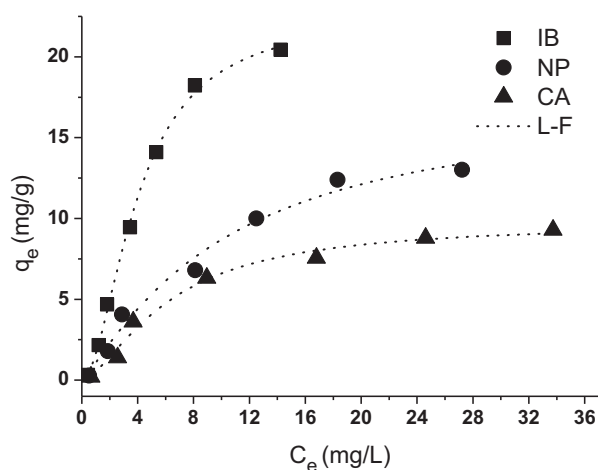

Fig. 2. Langmuir–Freundlich isotherm curve for PD adsorption.

provided in supplementary figure S2. The breakthrough time decreased with increasing flow rate because of the sufficient time for the adsorption process at lower flow rate, but not at the higher flow rate, and the ease with which the column bed became saturated. In case of IB adsorption, breakthrough occurred after 300 min at 3 ml/min flow rate. At the same flow rate, the breakthrough time was 180 and 120 min for NP and CA adsorption, respectively, which is lower than the breakthrough point found at the lower flow, which was discussed in the previous paragraph for the same condition.

The performances of breakthrough point for PD adsorption were observed at different RMC bed depths of 1.5 and 3.0 cm, keeping the flow rate and initial feed concentration constant at 1.5 ml/min and 10 mg/L (supplementary figure S3). For all three PD adsorptions, the breakthrough time was increased for higher bed length due to the increase in residence time. The breakthrough curve of the longer bed length took a longer time to get saturated, which increased the breakthrough time as well. For IB, breakthrough was observed after 1740 min at 3.0 cm bed length, which is higher than appeared at 1.5 cm bed length (840 min). In case of NP and CA adsorption, breakthrough appeared after 1680 and 1620 min for 3.0 cm RMC bed, respectively.

3.4. Estimation of adsorption parameters

The fixed-bed operational conditions strongly influenced the PD adsorption on the RMC bed. The important parameters of the process are adsorption capacity at breakthrough time (q_b), adsorption capacity at saturation time (q), length of mass transfer zone (MTZ) and fractional bed utilization (FBU). The amounts of PD retained in the RMC bed to the point of breakthrough (q_b) until saturation (q) were obtained by mass balance using the column data. The area under the curve ($1 - C/C0$) to the point of breakthrough is proportional to q_b and the saturation of the bed is proportional to q. Adsorption capacities at breakthrough and saturation time were calculated by Eqs. (4) and (5), respectively [34].

$$q_b = \left(\frac{C_0 Q}{1000m}\right) \int_0^{t_b} \left(1 - \frac{C}{C_0}\right) dt \qquad (4)$$

$$q = \left(\frac{C_0 Q}{1000m}\right) \int_0^t \left(1 - \frac{C}{C_0}\right) dt \qquad (5)$$

where Q is the volumetric flow rate (ml/min), m the adsorbent quantity (g), t_b the breakthrough time (min), t the bed saturation time (min), and C and C_0 are the final and initial PD concentrations. The values of adsorption capacities for IB, NP and CA adsorption on the RMC fixed-bed at breakthrough and saturation time were calculated and are presented in Table 5.

The ratio of q_b/q can be used to calculate MTZ according to Eq. (6).
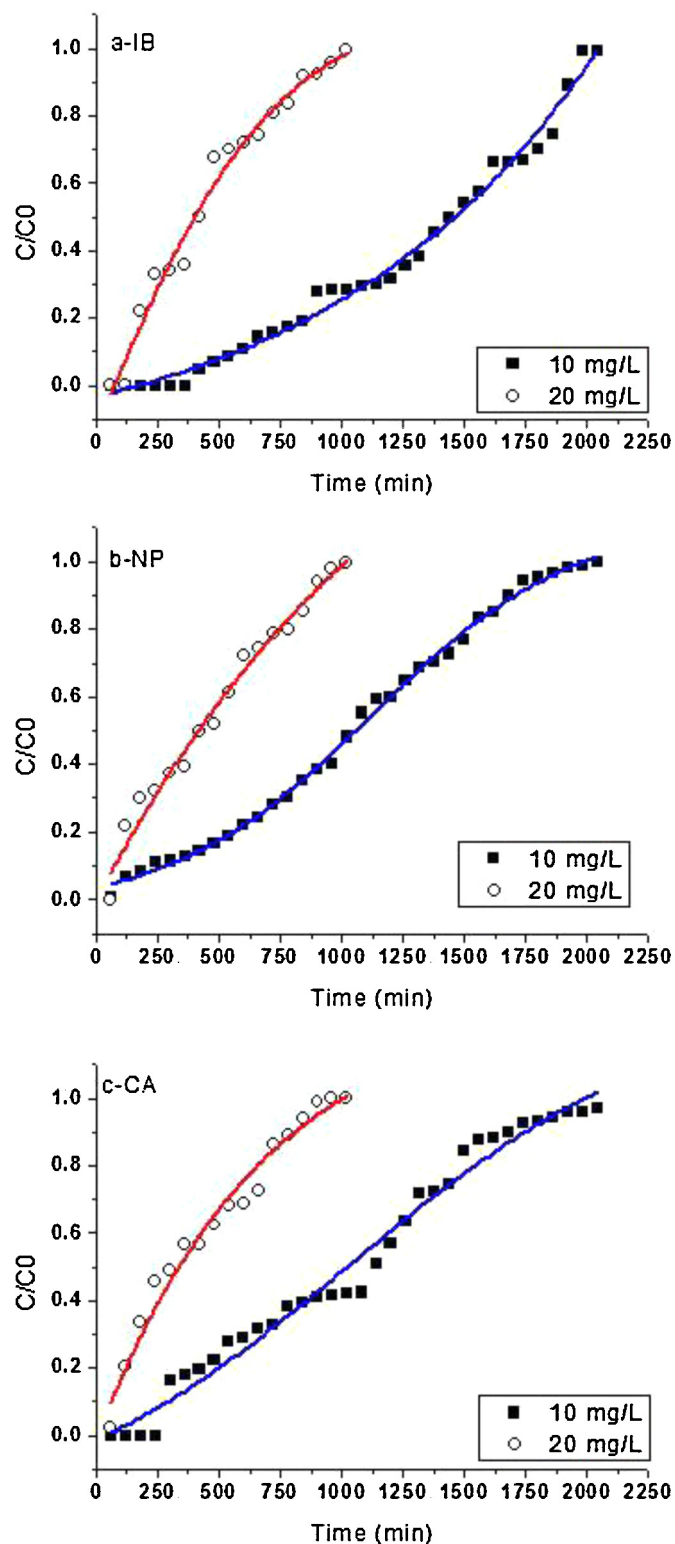
$$\text{MTZ} = \left(1 - \frac{q_b}{q}\right) D \qquad (6)$$

Fig. 3. (a–c) Breakthrough curve of (a) IB; (b) NP; and (c) CA adsorption at different initial PD concentrations.

Table 5
Adsorption capacities (q_b, q), MTZ and FBU values for PD adsorption.

PDs	Parameters	10 mg/L	20 mg/L	3 ml/min	3 cm
IB	q_b (mg/g)	14.551	4.537	9.337	30.300
	q (mg/g)	25.988	15.527	17.222	46.139
	MTZ (cm)	0.660	1.062	0.687	1.029
	FBU	0.559	0.292	0.542	0.657
NP	q_b (mg/g)	8.507	4.121	4.121	30.625
	q (mg/g)	19.355	15.452	15.505	46.295
	MTZ (cm)	0.841	1.099	1.101	1.015
	FBU	0.439	0.267	0.266	0.662
CA	q_b (mg/g)	6.669	2.132	2.030	29.629
	q (mg/g)	19.177	13.13	11.954	45.752
	MTZ (cm)	0.979	1.257	1.245	1.057
	FBU	0.348	0.162	0.169	0.648

3.5. Fixed-bed modeling of PD on RMC surface

Breakthrough curves were plotted by Eqs. (2) and (3) for the Thomas and Yoon–Nelson models at different initial feed concentrations, flow rates and bed depths for IB, NP and CA adsorption and their parameters. The Thomas rate constant (k_{th}), adsorption capacity (q_0), Yoon–Nelson rate constant (k_{yn}), and 50% breakthrough (τ) and correlation coefficients were determined from the curve and are presented in Table 6.

The adsorption capacity was decreased with increasing initial IB concentration from 10 to 20 mg/L. A similar effect was observed for the other PD. The higher concentration of solute occupied the available binding sites more rapidly and the remaining adsorbate inept to bind onto adsorbent surfaces. Thus, the amount of adsorbate adsorbed was decreased at increasing initial feed concentration. This was due to the fast breakthrough that occurred at higher initial feed concentration with lower treated volume since the higher initial feed concentration gradient caused a fast transport due to the increased mass transfer coefficient [33]. The slower transport gave the PD molecules sufficient time to bind to the adsorption active sites, thus increasing the adsorption capacity at lower initial feed concentration.

The adsorption capacity for PD adsorption on the RMC surface analyzed from the Thomas model (Table 6) showed a decrease as the volumetric flow rate was increased from 1.5 to 3.0 ml/min. The adsorbent surface was saturated easily with increasing volumetric flow rate, which decreased the velocity of the adsorbate passing through the adsorbent bed, thereby decreasing the adsorption zone. A sharp decrease in τ calculated from the Yoon–Nelson model has also been reported for PD adsorption with an increase in volumetric flow rate (Table 6).

Increasing bed depth of the column affects the breakthrough time for adsorption in a fixed-bed column. The adsorption capacity increased at higher bed depth, as the amount of adsorbent was kept constant. Columns of different diameter were used to vary the bed depth with the same amount of adsorbent. The increase in bed depth provides more active binding sites for the PD to get attached on the RMC surface. In addition, an increase in bed depth provides the more residence time to PD molecules to remain in contact with the adsorbent surface, thereby increasing the exhaustion of the adsorbent bed and hence increasing the adsorption capacity at higher bed height. The maximum adsorption capacity for IB adsorption was 48.576 mg/g, as calculated from the Thomas model at a bed depth of 3.0 cm, initial concentration 10 mg/L and flow rate 1.5 ml/min (Table 6).

3.6. Effect of pH on PD adsorption

Solution pH played a significant role in the adsorption process. Experiments were performed in the pH range of 3–9 (Fig. 4). The

The value of MTZ calculated from this equation is the maximum value that corresponds to the bed depth (D). As the mass transfer efficiency increases, the value decreases, eventually reaching the ideal condition where MTZ is zero and the breakthrough curve is a step function [34]. The values of MTZ for IB, NP and CA adsorption are presented in Table 5. The MTZ values are affected by the column parameter.

Table 6
Thomas and Yoon–Nelson parameters and model deviations at different operating conditions.

PDs	Model	Parameters	10 mg/L	20 mg/L	3 ml/min	3 cm
IB	Thomas	k_{th} (ml/mg min)	0.289	0.299	0.805	0.179
		q (mg/g)	28.149	17.084	19.364	48.576
		χ^2	0.003	0.004	0.004	0.001
		R^2	0.969	0.963	0.969	0.991
	Yoon–Nelson	k_{yn} (/min) $\times 10^{-2}$	0.289	0.597	0.805	0.179
		τ (min)	1407.458	427.092	484.079	2428.794
		χ^2	0.003	0.004	0.005	0.001
		R^2	0.969	0.962	0.967	0.990
NP	Thomas	k_{th} (ml/mg min)	0.305	0.243	0.592	0.216
		q (mg/g)	20.806	17.219	18.115	47.668
		χ^2	7.72E−4	0.003	0.004	6.388E−4
		R^2	0.993	0.968	0.965	0.995
	Yoon–Nelson	k_{yn} (/min) $\times 10^{-2}$	0.304	0.485	0.592	0.216
		τ (min)	1040.286	430.494	452.891	2383.411
		χ^2	7.70E−4	0.002	0.003	6.388E−4
		R^2	0.991	0.970	0.964	0.996
CA	Thomas	k_{th} (ml/mg min)	0.286	0.247	0.625	0.233
		q (mg/g)	20.507	14.336	13.399	46.532
		χ^2	0.003	0.005	6.083E-4	0.001
		R^2	0.973	0.943	0.993	0.992
	Yoon–Nelson	k_{yn} (/min) $\times 10^{-2}$	0.286	0.493	0.625	0.230
		τ (min)	1025.357	358.388	334.985	2326.612
		χ^2	0.002	0.004	6.083E−4	0.001
		R^2	0.970	0.934	0.992	0.993

surface of the adsorbent was highly influenced by the solution pH. Meanwhile, potentiometric titration of RMC revealed a pH_{zpc} of 5.48, which indicated that the surface charge of RMC changed from positive to negative from pH 3 to 9, with the neutral crossover at pH 5.48. The PD removal was maximum in the pH range of 3–5. The probable mechanism for PD adsorption on the RMC bed is presented below.

3.7. Mechanistic interpretation

3.7.1. Adsorbate characteristics
Adsorbate characteristics such as octanol-water coefficient and aqueous phase solubility play an important role in multi-component adsorption system and more hydrophobic PD adsorbs to a greater extent than less hydrophobic one.

3.7.1.1. Octanol–water partition coefficient of PD. The effective adsorption of PD on RMC surfaces may be understood in terms of the octanol–water partition coefficient (K_{ow}) [35]. Reportedly, if log K_{ow} is <2.5, the compound has a low adsorption potential (i.e.,

Fig. 4. Effect of pH on PD adsorption.

it does not adsorb and is not very lipophilic), if log K_{ow} is between 2.5 and 4.0, the compound has a medium adsorption potential and if log K_{ow} is >4.0, the compound has a high adsorption potential and is very lipophilic. The order of log K_{ow} reported for different PD is summarized in Table 1. IB has highest log K_{ow} with comparably lower solubility than CA. Hence, the adsorption of IB is higher on the RMC surface. The tendency of PD molecules to adsorb is a function of their affinity for water as compared to their affinity for the adsorbent. The adsorption generally increases as the adsorbate's solubility decreases [36]. The adsorption of IB, NP and CA were in good accord with their log K_{ow} (IB) > (NP) > (CA).

3.7.1.2. Weak-acidic character of PD. The three selected PD consist of a combination of non-polar/non-ionizable and polar/ionizable functional moieties. IB, NP and CA are weak carboxylic acid PD with ionizable groups. PD get stabilized by charge separation and charge delocalized resonating structures and have bipolarity due to carboxylic functional groups. The pK_a establishes the fraction of protonated and deprotonated form. The weak acidity of the PD is due to the hydrogen in the carboxylic group. PD molecules become dissociated into their corresponding carboxylate conjugate base and protons as the pH is increased above pK_a values. The pK_a of a monoprotic acid is the pH at which equal amounts of protonated and deprotonated compounds are present. At one pH unit lower than the pK_a, the functional groups exist predominately (>90%) in the neutralized form, while at one pH unit higher than the pK_a the functional groups exist predominately in the ionized form [37,38]. pH_{zpc} of the RMC was 5.48, showing that the RMC surfaces remained positive at pH lower than 5.48. The pK_a values of IB, NP and CA are presented in Table 1. At pH lower than the pH_{zpc} of RMC, all three weakly acidic PD had some deprotonated form ($\approx$10%) and were bonded with the RMC surfaces due to the electrostatic attractions, while the remainders ($\approx$90%) in unionized form were adsorbed due to the hydrophobic interactions.

3.8. Adsorbent characteristics

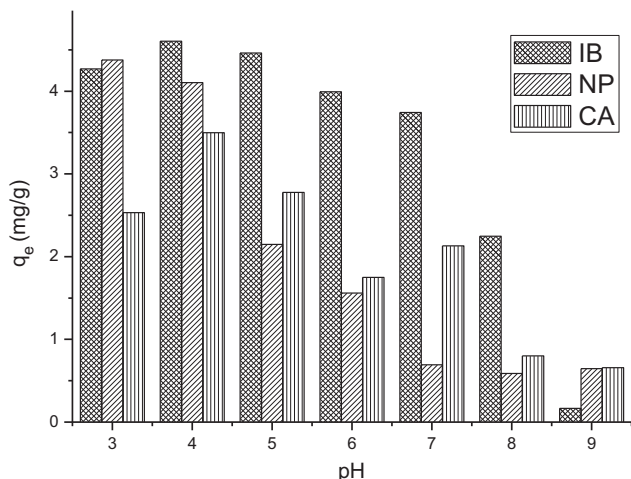The surface morphology and shape of the developed material was carbon-tubules rather than a typical activated carbon

structure. Additionally, a mesoporous material is regarded as good for adsorption [39,40]. We believe that being a mesoporous material, RMC not only allows adsorption at the surfaces but also inside the large pores and increases the adsorption capacity. Surface area (224.6 m^2/g) and pH$_{zpc}$ (5.48) played an affirmative role in the adsorption of the PD onto the RMC surface. In addition to that the difference in adsorption capacities was found between batch (IB; 22.672 mg/g) and column (IB; 28.149 mg/g) study under the same initial PD concentration (10 mg/L). One of the reasons for observed discrepancies between the batch and column systems can be due to presence of pores on the surface of RMC that enhanced solid state diffusion relative to the batch study [41].

The analysis of FTIR spectra showed characteristic IR bands of phenol-like compounds (3386/cm), aromatic rings weak band (757/cm) and overtone frequencies (1977 and 1608/cm), aliphatic hydrocarbons stretching vibrations (2918 and 2849/cm) and ketonic groups (1700/cm). An aldehydic group was confirmed with C–H absorption at 2849/cm and C=O absorption at 1700/cm. The weak, small but exposed absorption band at 2160/cm was attributed to conjugate diene moieties (–C=C–C=C–) obtained from vitamin-skeleton and/or unsaturated double bond structures (Table 3). Due to the diverse functional groups, the RMC surface showed 'variable charge active sites' (as a function of pH) and formed weak electrostatic forces for PD uptake on the RMC surface.

4. Conclusion

In this study, a simple but efficient strategy was developed to produce novel RMC with a mesoporous tubular structure using chemical and physical activation. Surface characteristics such as pH$_{zpc}$, mesoporosity, high surface area and surface-derived functional groups of RMC potentially make this material suitable for adsorption. The adsorption of three emerging PD (IB, NP and CA) was studied. Thomas and Yoon–Nelson mathematical models were applied to interpret the breakthrough properties. The adsorption capacities calculated from the Thomas model showed the highest adsorption for IB on the RMC packed fixed-bed column, which was attributed to high log K_{ow} and low aqueous solubility of IB. The weak-acidic character of PD and surface property of adsorbent also accelerated the adsorption of PD on the RMC surface.

Acknowledgements

Appendix A. Supplementary data

Supplementary data associated with this article can be found, in the online version, at doi:10.1016/j.jiec.2013.06.051.

References

[1] G. Mertxell, P. Mira, B. Damia, Analytical Chemistry 81 (2009) 898.
[2] O.P. Togunde, K.D. Oakes, M.R. Servos, J. Pawliszyn, Environmental Science & Technology 46 (2012) 5302.
[3] S.K. Ritter, Chemical Engineering News 84 (2006) 37.
[4] WHO, Pharmaceuticals in Drinking-water, WHO/HSE/WSH/11.05, 2011.
[5] E. Vulliet, C. Cren-Olive, M.-F. Grenier-Loustalot, Environmental Chemistry Letters 9 (2011) 103.
[6] X.S. Miao, B.G. Koenig, C.D. Metcalfe, Journal of Chromatography A 952 (2002) 139.
[7] L. Wang, G.G. Ying, J.L. Zhao, X.B. Yang, F. Chen, R. Tao, S. Liu, L.J. Zhou, Science of Total Environment 408 (2010) 3139.
[8] J.W. Kim, H.S. Jang, J.G. Kim, H. Ishibashi, M. Hirano, K. Nasu, N. Ochikawa, Y. Takao, R. Shinohara, K. Arizono, Journal of Health Science 55 (2009) 249.
[9] C. Nebot, S.W. Gibb, K.G. Boyd, Analytica Chimica Acta 598 (2007) 87.
[10] T.A. Ternes, Water Research 32 (1998) 3245.
[11] M.L. Farré, I. Ferrer, A. Ginebreda, M. Figueras, L. Olivella, L. Tirapu, M. Vilanova, D. Barceló, Journal of Chromatography A 938 (2001) 187.
[12] S. Öllers, H.P. Singer, P. Fässler, S.R. Müller, Journal of Chromatography A 911 (2001) 225.
[13] R. Andreozzi, M. Raffaele, P. Nicklas, Chemosphere 50 (2003) 1319.
[14] F. Stuer-Lauridsen, M. Birkved, L.P. Hansen, H.-C. Holten Lützhoft, B. Halling-Sorensen, Chemosphere 40 (2000) 783.
[15] T.A. Ternes, M. Meisenheimer, D. Mcdowell, F. Sacher, H.-J. Brauch, B. Haist-Gulde, G. Preuss, U. Wilme, N. Zulei-Seibert, Environmental Science & Technology 36 (2002) 3855.
[16] M. Petrovic, E. Eljarrat, M.J.L. De Alda, D. Barcelo, Trends in Analytical Chemistry 20 (2001) 637.
[17] I. Ali, V.K. Gupta, Nature Protocols 1 (2007) 2661.
[18] A.D. Dwivedi, K. Gopal, R. Jain, Chemical Engineering Journal 168 (2011) 1279.
[19] J.C. Crittenden, S. Sanongraj, J.L. Bulloch, D.W. Hand, T.N. Rogers, T.F. Speth, M. Ulmer, Environmental Science & Technology 33 (1999) 2926.
[20] C. Liang, Z. Li, S. Dai, Angewandte Chemie International Edition 47 (2008) 3696.
[21] Q. Sui, J. Huang, Y. Liu, X. Chang, G. Ji, S. Deng, T. Xie, G. Yu, Journal of Environmental Science 23 (2011) 177.
[22] K. Nakagawa, A. Namba, S.R. Mukai, H. Tamon, P. Ariyadejwanich, W. Tanthapanichakoon, Water Research 38 (2004) 1791.
[23] J. Liangliang, L. Fengling, X. Zhaoyi, Z. Shourong, Z. Dongqiang, Environmental Science Technology 44 (2010) 3116.
[24] S.P. Dubey, A.D. Dwivedi, K. Gopal, M. Sillanpää, Chemical Engineering Journal 165 (2010) 537.
[25] USDA, ARS, National Genetic Resources Program. Germplasm Resources Information Network – (GRIN), National Germplasm Resources Laboratory, Beltsville, Maryland, 2006 (last updated on 14/01/2006).
[26] N. Nakada, K. Komori, Y. Suzuki, Environmental Sciences 12 (2005) 359.
[27] A.C. Alder, A. Bruchet, M. Carballa, M. Clara, A. Joss, D. Löffler, C.S. McArdell, K. Miksch, F. Omil, T. Tuhkanen, T.A. Ternes, in: T.A. Ternes, A. Joss (Eds.), Consumption and Occurrence, 15, IWA Publishing, London, 2006.
[28] T.X. Bui, H. Choi, Journal of Hazardous Materials 168 (2009) 602.
[29] ASTM, Refractories; Carbon and Graphite Products; Activated Carbon, Annual Book of ASTM Standards, 1995 5.01.
[30] H.C. Thomas, Journal of the American Chemical Society 66 (1944) 1664.
[31] Y. Yoon, J. Nelson, American Industrial Hygiene Association Journal 45 (1984) 509.
[32] C.B. Lopes, E. Pereira, Z. Lin, P. Pato, M. Otero, C.M. Silva, A.C. Duarte, J. Rocha, Microporous and Mesoporous Materials 145 (2011) 32.
[33] Z. Aksu, G.F. Ferda, Process Biochemistry 39 (2004) 599.
[34] C.J. Geankoplis, Transport Process and Unit Operations, 3rd ed., PTR Prentice Hall, USA, 1993.
[35] D.C. Luehrs, T.N. Rogers, Correlation of the limiting partition coefficient of organic solutes between water and activated carbon with the octanol/water partition coefficient, in: Great Lakes Regional American Chemical Society Meeting, Normal, IL, May 20, 1996.
[36] Weber W.J.Jr., Physicochemical Processes, Wiley-Interscience, New York, 1972.
[37] D.G. Watson, Pharmaceutical Analysis: A Textbook for Pharmacy Students and Pharmaceutical Chemists, 2nd ed., Churchill Livingstone, Edinburgh, 1999.
[38] O. Lorphensri, J. Intravijit, D.A. Sabatini, T.C.G. Kibbey, K. Osathaphan, C. Saiwan, Water Research 40 (2006) 1481.
[39] V. Fierro, V. Torne-Fernandez, A. Celzard, Microporous and Mesoporous Materials 92 (2006) 243.
[40] M. Stacy, F. Pasquale, J. Mietek, Journal of the American Chemical Society 130 (2008) 15210.
[41] E. Lopez, B. Soto, M. Arias, A. Nunez, D. Rubinos, M.T. Barral, Water Research 32 (1998) 1314.